New Early Oligocene Zircon U-Pb Dates for the 'Miocene' Wenshan Basin, Yunnan, China: Biodiversity and Paleoenvironment

Yimin Tian[1], Robert A. Spicer[2,3], Jian Huang[2], Zhekun Zhou[2,4], Tao Su[2], Mike Widdowson[5], Linbo Jia[6], Shihu Li[7,8], Wenjian Wu[1], Li Xue[1], Penghui Luo[1], Shitao Zhang[1*]

[1]*Faculty of Land Resource Engineering, Kunming University of Science and Technology, Kunming, 650093, China;*

[2]*CAS Key Laboratory of Tropical Forest Ecology, Xishuangbanna Tropical Botanical Garden, Chinese Academy of Sciences, Xishuangbanna 666303, China;*

[3]*School of Environmental, Earth and Ecosystem Sciences, The Open University, Walton Hall, Milton Keynes, MK7 6AA, U.K;*

[4]*Kunming Institute of Botany, Chinese Academy of Sciences, Kunming 650201, China;*

[5]*Geology: School of Environmental Sciences, University of Hull, Hull HU6 7RX, U.K;*

[6]*CAS Key Laboratory for Plant Diversity and Biogeography of East Asia, Kunming Institute of Botany, Chinese Academy of Sciences, Kunming 650204, China;*

[7]*State Key Laboratory of Lithospheric Evolution, Institute of Geology and Geophysics, Chinese Academy of Science, Beijing 100029, China;*

[8]*Lancaster Environment Centre, Lancaster University, LA1 4YQ, Lancaster, U.K.*

*Corresponding author: Shitao Zhang (taogezhang@hotmail.com)

Abstract: The sedimentary basins of Yunnan, Southwest China, record detailed histories of Cenozoic paleoenvironmental change. They track regional tectonic and palaeobiological evolution, both of which are critically important for the development of modern floral diversity in southwestern China and throughout Asia more generally. However, to be useful, the sedimentary archives within the basins have to be placed within a well-constrained timeframe independent of biostratigraphy. Using high resolution U-Pb dating, we redefine the age of fossil-bearing strata in the Wenshan Basin. Regarded as Miocene for the last half century, these basin sediments encompass 30±2 and 32±1 Ma early Oligocene tuffaceous horizons thus indicating a significantly greater antiquity than previously recognized. Together with other regional age revisions, our result points to widespread Yunnan basin and orographic development, as largely having taken place by the end Paleogene. This age revision provides an important new perspective on the preserved biotas and their evolution in Yunnan, and especially our understanding of the origin of Asian biodiversity which, regionally, had a near-modern composition by the early Oligocene. Crucially, this revised age evidences late Eocene-early Oligocene regional tectonism, pointing to the rise of eastern Tibet and the Hengduan mountains before the growth of the Himalaya, and that Asia's high plant diversity has a Paleogene origin.

Keywords: U-Pb dating, Biodiversity hot spot, Paleoenvironment, Sedimentary basin, SW China

1 Introduction

The orographic development of the Himalaya and Yunnan acted as a cradle for modern Asian biodiversity, and greatly influenced the evolution of modern Asian climate including monsoon dynamics (e.g., Boos et al., 2010; Molnar et al., 2010;

Spicer et al., 2017, 2020a). However, understanding the links between topography, climate and biodiversity is entirely dependent on accurately dated regional geology. The India-Eurasia collision early in the Paleogene (see references in An et al., 2021), represents perhaps the most dramatic tectonic event of the Cenozoic, and one that has had far-reaching consequences for the entire planet (e.g., Molnar and Tapponnier, 1975; Yin and Harrison, 2000): Following this, the orography of Yunnan underwent significant change because the arrival of India led to predominantly northward compression and the eastward and southward extrusion of parts of the Qiangtang Terrane (Tapponnier et al., 1982; Li et al., 2020a), which today forms large parts of eastern Tibet and the Hengduan Mountains in Yunnan. The accompanying deformation throughout Yunnan created more than 150 Cenozoic sedimentary basins (Huang et al., 2016b), but because many, including the Jinggu and Wenshan basins lack good radiometric age constraints, the timing and processes underlying Yunnan's tectonic evolution and associated paleoenvironmental changes have hitherto remained poorly understood.

Until recently many of the basins hosting mainly lacustrine-marsh facies were considered to be of Miocene age (YBGMR, 1990), but excavations during infrastructure development and coal mine operations have revealed hitherto hidden details. In the past few years, the geochronology of supposedly Neogene sediments within several basins (e.g., Jianchuan, Lühe and Markam Basins), has been revised using radiometric dating, and all have been shown to be Paleogene (Ma, 2013; Gourbet et al., 2017; Linnemann et al., 2017; Su et al., 2019; Li et al., 2020b; Zheng et al., 2020), thus raising questions regarding the antiquity of other similar basins throughout the region.

The Eocene-Oligocene (E-O) transition represents one of the most important global climate and biosphere changes in the past 66 million years since it marks a step change in the transition from a 'hothouse' to an 'ice house' world; the deep-sea record, carbon and oxygen isotope perturbations reflect numerous Earth system responses worldwide since the Oligocene (e.g., Zachos et al., 2001). Yunnan is an area hosting one of the most important modern global biodiversity ‘hotspots' (Myers et al., 2000), and has been the focus of much geological, ecological and phylogenetic research, therefore, with recent age revisions its sedimentary record can offer new insights into low latitude environmental changes across this globally important interval.

Here we focus on a classic ‘Miocene’, predominantly lacustrine, basin in SE Yunnan containing abundant fossils (including leaves, fruits, pollen, fishes, and molluscs), and revise the age of its deposits using (U-Pb) zircon dating. These ages help constrain a more robust timing for the tectonic development of SE Yunnan, especially its paleoenvironmental history encompassing palaeoclimate, palaeogeography, palaeobiology and, ultimately, what it can then reveal about the history of Asian biodiversity development.

2 Geological Setting

2.1 Geological background

The development of the Dushitou Village section in northwestern Wenshan Basin (23°24'36″-23°25'21″ N, 104°12'39″-104°13'44″ E, 1272-1430 m), southeastern Yunnan, southwest China, was controlled by movement on the Wenshan-Malipo fault – part of the South China fold system (Figs. 1, 2 and 3). Early research named the extensive basin infill sediments the Huazhige Formation, and these were then regarded as being Neogene in age (YBGMR, 1990). Subsequently an early-middle Miocene age was assigned because of a seemingly conformable contact between the Huazhige Formation and the underlying Yanshan Formation, dated as late Oligocene (YBGMR, 1990). Towards the end of the last century, a regional geological survey concluded that these two formations were in fact unconformable and, based on lithostratigraphic and biostratigraphic characteristics as well as regional correlation, that the Huazhige Formation may be age-equivalent to the middle-upper Miocene Xiaolongtan Formation (YBGMR, 1990). Subsequently, palaeomagnetic analysis offered an age range of 15.2~16.5 Ma for a section near Dushitou Village, but the sampled outcrop was not sufficiently extensive (~270 m), and thus only covered about one third of the Huazhige Formation thickness (Lebreton-Anberrée et al., 2016); further, it lacked radiometric tie points and index fossils and thus lacked the robust dating constraints required for more sophisticated interpretation.

We recently discovered two volcanic ash layers in the Dushitou Village section in sediments assigned to the Huazhige Formation (YBGMR, 1990). These are located 600 m apart laterally, and are stratigraphically separated by 49.6 m (Fig. 4). Henceforth these are referred to as 'Ash 1' (23°14'54″ N, 104°12'36″ E, 1292 m) and 'Ash 2' (23°24'95″ N, 104°12'12″ E, 1301 m). Note that Ash 1 occurs at a higher stratigraphical level than Ash 2. The Dushitou Village section spans the whole Huazhige Formation, is capped by Quaternary sediments, and overlies the Yanshan Formation. The section comprises greyish, beige, light fawn mudstones and muddy siltstones together with greyish-yellow sandstones, and contains abundant, well-preserved plant fossils in key horizons (Fig. 4). It was initially interpreted to be composed of sediments deposited in a lacustrine-paludal environment, but is now known to expose dominantly lacustrine-fluvial facies with limnic ostracods.

Accordingly, our work concentrates on the age of the Wenshan flora based on U-Pb dating of zircons within volcanic ashes preserved as part of the lacustrine succession.

2.2 Plant Fossils of the Wenshan Basin.

The Wenshan Basin has long been known to contain a fossil biota that is both abundant and taxonomically diverse. Numerous freshwater fish fossils (e.g., Cyprinidae), and insect fossils, (e.g., Diptera and Hymenoptera), are accompanied by 32 pollen types, including those of Fagaceae and Juglandaceae, and more than 60 species of plant megafossils (e.g., Meng et al., 2014; Li et al., 2015; Huang et al., 2016a, 2017, 2018). Recent new collections have expanded this diversity, and according to a preliminary census, the flora includes ferns (1 family 1genus 1 species), gymnosperms (2 families 5 genera 11 species) and angiosperms (50+ families 92+ genera 200+ species) (Fig. 7 and Table. 1). Identification of the plant fossils making up the highly diverse palaeoflora is ongoing.

Many of the taxa, at least at genus level are similar to those found in the region today (Table 1), and partly as a consequence of this apparently modern aspect the flora has been regarded as Miocene in age (YBGMR, 1990; Lebreton-Anberrée et al., 2016).

3 Sampling, methods and results

The volcanic ash samples were collected from the northern Wenshan Basin, a site that has yielded plant fossils from several horizons referred to collectively as the 'Wenshan flora' (Fig. 4). The volcanic ash beds are intercalated with the fossiliferous layers, such that the age of the ashes can be used to radiometrically date the Wenshan flora.

3.1 Field characteristics of ash layers

Ash 1 occurs as intermittent lenses, typically 2-10 cm thick, and more than 20 m in lateral extent; it consists of two distinct layers of brown coarse volcaniclastics (< ~10cm apart), and set within light grey massive, to weakly laminated clays/silts. Inspection of these lenses reveal evidence of sedimentary structures (i.e. no cross-bedding), but they do display graded bedding, typically becoming somewhat coarser toward the center of the lens (Fig. 5a, b), while other lenses exhibit marked upward fining (Fig. 5b). Individual grains are extremely angular and heterolithic, but the horizons themselves also encompass small amounts of clay and silt.

'Ash 2' is similarly brown in color, typically 3-4 cm thick, but differs from the lower example in that it is more laterally continuous, and its constituent volcanogenic grains more euhedral. Inspection reveals an internal structure: Its basal layer (~1.5 cm), comprises volcanic ash grains, and the lower contact with the underlying light grey clay displays small 'loading structures' likely resulting from 'dumping' onto a soft, semi-liquid lacustrine substrate. The light clay immediately beneath this lower contact is stained brown – probably an eluviation phenomenon by iron-bearing groundwater. The upper layer of 'Ash 2' (0.6 cm), is a finer. darker brown clay-like material with well-defined upper and lower contacts (Fig. 5e, f).

3.2 Thin section and zircon morphologic analysis

Whole rock thin sections were examined using a Leica DM2700 P petrographic microscope at the Laboratory of Geological Environment, Kunming University of Science and Technology, and imaged with Leica Application Suite (LAS) software. Samples were composed of minerals and lithic fragments typical of sedimented volcaniclastic rocks (Fig. 5). The mineral fragments were mainly composed of quartz for both 'Ash 1' and 'Ash 2', with admixes of K-feldspar (i.e., sanidine - low birefringence crystals lacking lamellar twinning), and plagioclase for 'Ash 1', and sanidine and primary 'igneous' biotite for 'Ash 2'. Quartz crystals were mostly irregular and angular, some cuspate , and some had obvious internal fracturing. K-feldspar and plagioclase grains were typically platy or tabular, sub-angular, and non-turbid.

3.3 Zircon separation

Samples were crushed and disaggregated, then crushed using a jaw-crusher followed by a double roll crusher; this crushate was then washed by table concentrator. Samples visually identified to contain a significant high heavy mineral content were further crushed to release individual grain sizes, and then zircon grains were separated using magnetic, electromagnetic techniques, and heavy liquid separation. The resulting sample aliquots were further sorted by hand using an optical petrographic microscope. Zircon grains were then hand-picked and set in an epoxy mount, which was then polished to expose the interiors of the crystals ready for imaging by optical and cathodoluminescence (CL) techniques. These mounts were subsequently re-polished to EBSD (Electron Back - Scattered Diffraction) standard using colloidal silica, and carbon coated. A Tescan MIRA 3 field emission scanning electron microscope (SEM; 7 KV voltage, 17 mm working distance) at Beijing Zhongke Kuangyan Test Technology Co., Ltd, was used to collect detailed CL images of individual zircon grains (Fig. 6).

Inspection reveals that zircon grains of ‘Ash 1’ are dominated by mostly colorless, short prismatic forms (Fig. 6) with lengths ranging from 70 μm to 250 μm; length: width (L: W) ratios are 1:1 to 2:1. A small population are light brown, have a pyramid shape, and are broken or cracked on the surface, indicating mechanical abrasion; others are rounded to elliptical thus indicative of transportation. The zircon images revealed a fine oscillatory zoning typical of magmatic zircon (Fig. 6), which reflect changing conditions in the magma chamber. In some instances 'inherited' cores suggest more complex magmatic histories, and for these types of grains, laser spots were positioned on the zoned part, rather than the core, thus representing the most recent magmatic growth.

The zircon grains of 'Ash 2' are colorless, transparent and prismatic; the lengths range from 80 μm to 250 μm with length: width (L: W) ratios of 2:1 to 4:1. The majority of these grains are obviously euhedral with clear oscillatory zoning and, accordingly, are considered wholly indicative of primary magmatic growth. this few revealing 'inherited' cores were excluded from further analysis (Fig. 6).

No metamorphic features were identified in any zircon grains, and these minerals are thus interpreted to be of primary magmatic origin.

3.4 U-Pb ages of the Wenshan Basin

Analysis was carried out using on an Agilent 7500a ICPMS using LA-ICP-MS at the State Key Laboratory of Continental Dynamics in Northwest University, Xi'an, China. The laser spot size was 43 μm (10 Hz) on single ablation sites, and data acquisition employed peak jumping with standing times of 15 ms for ^{204}Pb, ^{206}Pb, ^{207}Pb, ^{208}Pb, and 10 ms for Th and U: The resulting data was processed by means of ICPMSDataCal (ver 11.8) software, and Isoplot 3.0 graphics suite (Liu et al., 2010).

Zircon reference material 91500 was used as the external standard for calculating ages (Wiedenbeck et al., 2004), whilst NIST SRM 610 (external standard) and ^{29}Si (internal standard) were used to calibrate elemental content. Relative dating deviations for single spot analysis and weighted average age are respectively less than 2.2% and 0.6%.

Ash 1: Thorium (Th) content of fifty zircons in 'Ash1' samples ranged from 16.9 to 2209.0 ppm, with an average of 457.9 ppm: Uranium (U) content ranged from 34.6 to 2269.0 ppm, with an average of 474.9 ppm (Table S1). Accordingly, the ratio of Th to U is between 0.59 and 5.48, with all ratios exceeding 0.5; a value characteristic of magmatic zircon (Hoskin, 2000).

A total of fifty $^{206}Pb/^{238}U$ dates were obtained ranging in age from 28±1 Ma to 2543±28 Ma. Several age populations are present, but effectively form two distinct groups. Group (1): Those of Triassic to Paleoproterozoic age, where the zircon grains were either comparatively rounded or exhibited overgrowths, and are thus typical of 'inherited' and detrital zircon populations (Table S1), and Group (2), which represents a younger age group that returned a tight cluster of entirely Cenozoic ages (Table. S1; Fig. 6). Of these, 13 samples yielded a youngest mean age of 30±2 Ma with a MSWD value of 3.9, and a probability value of 0.000 (Fig. 6). However, CL images revealed the color of seven of these zircons as being somewhat lighter, and the associated concordant ratios of these young Cenozoic samples were lower than 90%, thus indicating U-poor and Pb-poor compositions (Fig. 6). Therefore, to further refine the returned age data, these seven were next excluded yielding a final mean age of 30±2 Ma from the remaining 6 samples.

Ash 2: Thorium (Th) content of thirty-nine analysed zircons in from 252.7 to 2528.6 ppm, with an average value of 703.2 Uranium (U) content ranged from 367.7 to 1450.4 ppm, with a mean of 740.1. The U/Th ratio for these is 0.49 ~ 1.74 with a 0.90 mean value; again, typical of magmatic zircon. A total of $^{206}Pb/^{238}U$ dates were then obtained ranging from 31±1 Ma to 217±5 Ma, including seven samples from late Triassic to early Paleocene, and 32 with exclusively late Paleogene ages (Table S1). After deselecting those with low concordant (<90%) results from the late Paleogene group, we obtained a final mean age of 32±1 Ma (Fig. 6).

Based on their characteristics we interpret ‘Ash 1’ and ‘Ash 2’ as representing primary air-fall deposition into the Wenshan palaeo-lake. However, ‘Ash 1’ is laterally discontinuous and although it shows graded bedding consistent with that produced as eruptions progress, and contains typical parallel bedding such as produced by still water deposition; accordingly, it contains some admixed lake sediments. We discount significant secondary reworking after deposition, but some local slumping/seismic disturbance may have taken place post-deposition while the sediments were still unconsolidated, and this may have given rise to the lenticular nature of the beds. The internal composition of ‘Ash 1’ and the broad age range of the zircons suggests significant mixing from several sources (Fig. 6). Significantly, ‘Ash 2’ is much finer grained and more continuous laterally. It also displays no clearly visible sedimentary structures or mixing with the lake clays such as would occur during reworking within the lake system, or influx from surrounding country rocks during flood event.

Despite their smaller size, the angularity of the grains and overall compositional and tighter age distribution of the zircons in Ash 2 suggests no significant sedimentary reworking/fluvial transport prior to final deposition. Therefore, its lateral continuity, structure and composition indicate that it is a primary ash, meaning the age of the youngest zircon populations from concordant grains (higher than 90%) represent the age of the entombing lake sediments (Fig. 5 and Table S1).

In effect, both Ash 1 and 2 reveal youngest 'magmatic' ages of between ~32 – 30 Ma, thus placing these two explosive magmatic events firmly within the Rupelian stage of the Oligocene, and providing key absolute dating horizons within the Huazhige Formation.

4 Discussion

4.1 Sedimentary environment

Lacustrine sedimentary successions are useful for reconstructing environmental/vegetation/landscape change in continental interiors because of their broad geographical coverage, sediment accumulation, and potential for high-resolution stratigraphy (e.g., some varved sediments record seasonal change) (Wang and Li, 1991).

Lithological and sedimentary features allow us to divide the Huazhige Formation into two sedimentary successions, and we respectively name them here as HZG-1 and

HZG-2, where HZG-1 underlies HZG-2. Each of these can then be further separated into two or three subsidiary successions as detailed henceforth (Fig. 4).

HZG-1 (93.5 m in thickness) is in unconformable contact with the underlying Yanshan Formation, and divided into three subsidiary successions named here as HZG-1-a (12.6 m thick), HZG-1-b (8.4 m thick), HZG-1-c (72.5 m thick).

HZG-1-a consists of a thick layer of light gray and off-white siltstone, silty mudstone and mudstone. The weathering surface and interlayers are greyish-yellow due to penetration by iron-bearing groundwater. Horizontal bedding is well developed and there are many laminae formed by differences in particle size and organic matter content, indicative of typical quiet-water lacustrine deposition with minimal flow and seasonal turnover. Numerous well-preserved fossils occur in this succession, including fish and plants. Some representative taxa include *Bauhinia* sp., *Burretiodendron* spp., *Cephalotaxus maguanensis*, *Exbucklandia acutifolia* (Huang et al., 2017), Fagaceae spp., Lauraceae spp., *Liquidambar maomingensis*, *Mahonia mioasiatica* (Huang et al., 2016a), *Mallotus* sp., *Rosa fortuita*, *Semecarpaphyllum* sp., *Sequoia maguanensis* and *Zelkova ningmingensis*. The source vegetation type is interpreted to have been subtropical evergreen broad-leaved forest, with some tropical components and taxa representative of vegetation typically growing on limestone (karst vegetation).

HZG-1-b includes one river sediment facies, and is composed of riverbed and floodplain sediments. Channel deposits are represented by a gray sandy conglomerate and pebbled sandstone at the bottom of the succession. Grain diameters range from 2-

30 cm and decrease in size gradually from bottom to top. Well-rounded gravel clasts occur near the bottom and are imbricated indicating the direction of water flow. The top part grades to a light grey and off-white mudstone, siltstone and silty mudstone with more or less horizontal bedding. Numerous fossil fragments occur, such as those of bivalves, ostracods and gastropods, indicating a return to low energy conditions. We regard the lower half of the fluvial succession as representing riverbed deposits and the upper half as representing floodplain deposition. The HZG-1-b succession is representative of one short lived fluvial episode, before the basin returned to hosting a large lake.

HZG-1-c is a succession composed of a thick layer of gray and off-white siltstone, silty mudstone and mudstone with horizontal and undulose bedding, hosting abundant fossil fragments, such as bivalves, ostracods, gastropods and numerous plant fossil fragments. Just above the midpoint of this succession many Cyprinidae fossils occur together with abundant plant fossils including leaves, fruits and flowers. This horizon has sourced most species of the Wenshan flora. We have recovered more than 5000 plant fossil specimens from this layer. The upper part of this succession hosts volcanic 'Ash 2', and some tawny and brown limonite beds, Fe nodules with a concentric circular structure and pseudomorphous limonite (limonite with pyrite crystals), which we interpret as being produced by a short-term oxidation event during a low water stage.

The HZG-2 succession begins with the appearance of a sandy conglomerate and pebble sandstone, indicative of another fluvial rejuvenation event, resting on the underlying HZG-1 (Fig. 4). This succession is divided into two secondary successions named as HZG-2-a (25.8 m thick) and HZG-2-b (41.6 m thick).

HZG-2-a is highly similar to HZG-1-b. However, there are three fluvial sediment packages within HZG-2-a and not just one as with HZG-1-b.

HZG-2-b is similar to HZG-1-c, and represents typical lacustrine sedimentation. A particularly significant component of this succession is the presence of 'Ash 1', and it also preserves numerous plant fossil taxa such as *Acer liquidambarfolium*, *Ailanthus confucii*, *Bauhinia wenshanensis* (Meng et al., 2014), *Calocedrus shengxianensis*, *Carpinus* sp., *Cornus* sp., Fagaceae spp., Lauraceae spp., *Mallotus* sp., *Palaeocarya hirta*, *Platycarya* sp., *Zelkova ningmingensis*. Compared with those of HZG-1-a, the plant composition was more similar to modern Wenshan, and suggests the climate was cooler than HZG-1-a, but still warm and humid.

Combining these successions, we find that at the start of deposition the early Oligocene Wenshan Basin hosted a lake, which transformed to a fluvial system as the water level fell, and then returned to a lake. When the basin restarted filling at the beginning of HZG-2-a, it experienced some significant environmental fluctuations because lacustrine deposition was punctuated by three fluvial events, and at times the lake depth became very shallow. Finally, the record of sedimentation ceased at the top of the preserved section. These quite marked changes in the depositional environment are not matched by obvious changes in the vegetation..

4.2 Implications for modern Asian biodiversity

4.2.1 The Wenshan Flora - one of the most diverse Paleogene floras known worldwide

Today, southwestern China is a major global biodiversity hotspot (Myers et al., 2000), and Cenozoic floras from this area have been studied extensively for the past seventy years in an effort to understand when and how such high biodiversity evolved. The fossil floras studied include the Shuanghe and Lühe floras of late Eocene to early Oligocene age, the Shuitangba, Mangdan, Xianfeng, Sanzhangtian, Shengli floras currently assigned to the mid-late Miocene, and the Tengchong, Yongping and Lanping floras of Pliocene age (for references see Huang et al., 2016b). Encompassed within these fossil floras are more than 53 families, 98 genera and 212 species, excluding the ongoing systematic study of the Wenshan flora which is emerging as one of the most diverse palaeofloras in south and central China, and is globally exceptional.

Not only is the fossil flora of the Wenshan Basin extremely rich (more than 200 species), most of the taxa can be assigned to modern genera (Table 1) despite the early Oligocene age. On a global scale, only a few floras display comparable diversity to that of Wenshan. These are the middle Eocene Green River flora (Brown, 1962) of western North America, the Middle Eocene Messel flora (Collinson, 1988) of Germany, and the Miocene Shanwang flora (Hu and Chaney, 1940), China. The abundant fossils within the different horizons of the Huazhige Formation, are well-preserved, and often possessing cuticle, which affords secure identification. Of note is that this Oligocene flora contains taxa that today are found in both tropical and subtropical climates, as well as in specialized limestone karst environments. Most abundant are typical subtropical forest elements such as Fagaceae, Lauraceae and Hamamelidaceae, which dominate in terms of the number of species, and Fagaceae as the most abundant family. Some tropical components such as *Burretiodendron*, *Iodes* and *Caryodaphnopsis* also occur. By comparison with the subtropical evergreen broad-leaf forest of modern Wenshan, the vegetation represented by the fossils seems to be in transition from tropical to subtropical and so, considering global warmth in the late Paleogene, was slightly warmer than today. This transitional status is also consistent with some degree of cooling from the Eocene to the early Oligocene. Moreover, numerous taxa typical of modern vegetation growing on limestone (karst vegetation) are present, such as *Bauhinia* (Meng et al., 2014), *Burretiodendron*, *Berhamniphyllum* (Zhou et al., 2020), *Ficus* (Huang et al., 2018), *Ulmus*, *Rosa*, *Zelkova* and *Carpinus*. Overall, it is clear that early Oligocene plant diversity at the generic level in southwestern China was not inferior to that of today.

Both the Wenshan flora and that of modern Yunnan exhibit exceptionally high diversity. Moreover, the compositions of early Oligocene floras of Yunnan, exemplified by the Lühe flora (Linnemann et al., 2017) in central Yunnan and the Wenshan flora in SE Yunnan, are remarkably similar to that of modern Yunnan. With local Miocene floras (Huang et al., 2016b) also displaying high levels of similarity to this early Oligocene flora it appears that floristic composition in this region has persisted for at least 32 million years. This complicates the use of plant biostratigraphy, whether palynological or megafossil-based, when trying to date

Cenozoic strata in the region. Recent radiometric dating in the Jianchuan Basin, the Lühe Basin and the Markam Basin (Ma, 2013; Gourbet et al., 2017; Linnemann et al., 2017; Su et al., 2019; Li et al., 2020b; Zheng et al., 2020), have consistently re-assigned the ages of fossil-bearing sediments from the originally stated middle-late Miocene to a late Eocene-early Oligocene age. This suggests strongly that modern-type vegetation was widespread in the region before the Neogene and, most significantly, indicates a Paleogene origin of Asian biodiversity.

4.2.2 The onset of modern floral diversity in Southern China

The modern East Asian flora may be divided into a Sino-Japanese Floral Region and a Sino-Himalayan Floral Region (Wu et al., 2006). The Red River-Ailao Shan fault zone forms a natural boundary between these two floral regions within Yunnan because its distinctive tectonics has given rise to a special physical geography, pronounced climatic differences on eastern and western slopes, and a floristic boundary called the Takana Line (Wu et al., 2006). To the west of this line the unique and extreme tectonic history of Tibet and the Himalaya has influenced both climate (Boos and Zhiming, 2010; Molnar et al., 2010) and biotic evolution (Favre et al., 2015; Spicer et al., 2017; 2020a). During the Neogene, the establishment of high elevations across what is now the Tibetan plateau (reviewed in Spicer et al., 2020a), and development of high elevations in the Himalaya (Ding et al., 2017), coupled with global cooling, produced a distinctive Sino-Himalayan flora. Some elements of the Sino-Himalayan flora seem to have migrated across to join the Sino-Japanese flora, which is largely conservative (Wu et al., 2006) possibly due to less dramatic tectonics and a stable latitudinal position.

The Wenshan early Oligocene flora is markedly different to the age-equivalent Lühe flora. Some of this disparity may be due to a difference in paleoelevation, but this is likely to be less than 1.8 km, the elevation of Lühe today, because although the palaeoelevation of the Lühe Basin is poorly constrained at the moment (Hoke, 2018), it is unlikely to have been significantly higher than its present elevation. Compared to Lühe flora, the Wenshan flora exhibits both tropical and typical limestone-loving taxa, such as *Liquidambar*, *Burretiodendron*, *Ficus* (Huang et al., 2018), and *Berchemiphyllum* (Zhou et al., 2020), and lacks those typical of cooler climates like *Picea* and *Tsuga*. The modern vegetation surrounding the Wenshan and Lühe fossil sites also show this difference. Given the age of Lühe flora it may represent an early phase of the Sino-Himalayan Flora that did not fully develop until the uplift of the Himalaya in the Miocene (Ding et al., 2017) and late Cenozoic cooling (e.g., Zachos et al., 2001).

What also attracts our attention is that *Coriaria japonica*, living in the Wenshan karst region during the Oligocene, is replaced by the forest-living species *C. nepalensis* in modern times. At the same time, *Pinus massoniana* and *Exbucklandia tonkinensis* are replaced separately by P. *yunnanensis* and *E. populnea*. Clearly some evolutionary change has taken place, but at the sub-generic level, and Wenshan Flora was already displaying features seen in the modern Sino-Japanese Flora by the early Oligocene (e.g., Huang et al., 2017).

Several Oligocene floras have been found and reported in southern China, such as in the various basins of Maoming, Guangdong, Ningming and Nanning, Guangxi, and Changchang, Hainan, Hoane Bo, Vietnam (e.g., Yao et al., 2009; Herman et al., 2017; Jin et al., 2017), all of which display similar floral composition and vegetation types as those of today. The ages of these South China and North Vietnam floras are mainly constrained by animal fossils, plant fossils (especially pollen fossils) and stratigraphic correlation, but absolute age determinations are lacking. The new precise age constraints on the Wenshan flora offers more secure evidence regarding the time of origin of the modern Sino-Japanese Flora, which appears to have been before the early Oligocene, most likely in the later Eocene.

4.3 Implications for the Tectonic Evolution of SE Tibet and Yunnan

During the early Paleogene, the collision of India with the Eurasian plate closed the Neotethys ocean seaway (An et al., 2021), and marine conditions regressed from southern Tibet and southwest Yunnan (Zhang et al., 2010). Inheriting a complex topography from earlier terrain collisions (Spicer et al., 2020b), the area of Tibet absorbed more than 90% of the relative plate motion between India and Eurasia (Wang et al., 2001) in the form of significant deformation and extrusion, primarily of the Qiangtang Terrane eastwards (Kapp et al., 2007).

Several Cenozoic intermontane basins formed in Yunnan and Vietnam in the late Eocene and early Oligocene and sediments from these basins reflect the paleoenvironmental changes over time. Our new date constraints for the Wenshan

Basin sediment fill is remarkably similar to those of recently re-dated sediments within the Jianchuan (e.g., Ma, 2013; Gourbet et al., 2017; Zheng et al., 2020), Lühe (Linnemann et al., 2017; Li et al, 2020) and Markam (Su et al., 2019) basins, thus pointing to widespread tectonic deformation of eastern Tibet, Yunnan and northern Vietnam, and simultaneous basin formation in the late Eocene and early Oligocene.

Based on drainage capture events of the Red River, especially the loss of drainage from the Yangtze Craton indicating Eocene gradient changes, Clift et al. (2006, 2020) suggested uplift across eastern Tibet and Yunnan likely took place before or during the Oligocene. The modern Red River, follows the Red River Fault Zone (Li et al., 2020a, 2020b), and seems to have become established in its near modern form almost immediately after the major Ailao Shan-Red River shear zone started moving ~ 35 Ma (e.g., Schärer et al., 1994).

This concurrent basin formation, as well as major surface uplift in the eastern Tibet area that began in the latest Eocene (Zheng et al., 2020), implies a common cause: The most obvious overall driving mechanism for landscape evolution in Yunnan is an Eocene south-north compression across Tibet and east and southeastwards extrusion of the Qiangtang terrane. We envisage propagation of deformation progressing from eastern Tibet into Yunnan triggering movement along major faults such as the Ailao Shan-Red River system. This is consistent with a detailed palaeomagnetic study of the Gonjo Basin within the eastern Qiangtang Terrane (Li et al., 2020b), which suggests a major deformation and 30° clockwise rotation of eastern Tibet between 52 and 48 Ma coincidental with more widespread deformation across Tibet and a slowdown of India's northward motion (Li et al., 2020a). Recent work indicates uplift of the Gonjo Basin (~ 100 km northwest of Markam) began in the early Eocene, rising from ~ 700 m to 3800 m, and that it had reached its modern elevation by the middle Eocene (Xiong et al., 2020). The nearby Markam Basin achieved its modern elevation in the earliest Oligocene, and soon after deformation progressed across Yunnan (Su et al., 2019). Recent dating and structural analysis of the Lühe Basin suggests that it was created by the onset of movement along the transpressional Chuxiong Fault at ~ 35 Ma, also concurrent with the start of movement on the Red River -Ailao Shan fault system (Li et al., 2020b).

To summarise, this tectonism drove the orographic evolution of the eastern and southeastern margins of Tibet, including NW Yunnan (Li et al., 2020a) and western Sichuan, and must have impacted the topography of SE Yunnan. The evolution of drainages reveals a strong, concomitant tectonic uplift in southern Tibet, including parts of the Gangdese, western Sichuan and eastern Yunnan during the late Eocene and early Oligocene (Clift et al., 2006; Yan et al., 2012).

5 Conclusions

The revised early Oligocene age for the Wenshan Basin sediments has profound implications for regional tectonics and biodiversity evolution. It now appears that Wenshan basin formation and subsequent sediment infill took place simultaneously with other basins development in eastern Tibet and elsewhere in Yunnan, and at the same time as major drainage reorganization. This strongly suggests a common driver in the Eocene and early Oligocene, and we would expect other basins in Yunnan, even extending into Vietnam, to have formed near simultaneously; this then raises doubts regarding the accepted, predominantly Miocene ages of many other regional basin fill and entombed palaeobiotas. It follows that additional absolute dating of the different numerous Cenozoic basins throughout the region is now required if we are to more fully understand the evolution of the region's topography, climate and biodiversity.

As with the Lühe, Markam and Jianchuan basins the modernity of the biota in the Wenshan Basin is clear, but has here been shown to be of early Oligocene age instead of Miocene. It is therefore now indisputable that the origin of one of the world's great biodiversity hotspots dates back to the Paleogene, and in southwestern China is not connected to Neogene tectonics. This contrasts with a Miocene age for diversification of Chinese plant lineages as inferred from molecular phylogenetic studies (Renner, 2016), and invariably linked to supposed 'uplift of Tibet' at that time (e.g., Lu et al., 2018). Such a straightforward concept now seems unlikely, and that the evolution of Tibetan topography was actually more protracted and complex (Spicer et al., 2020 a and b). If this Miocene diversification is real, drivers other than simple surface uplift are required as an explanation.

Acknowledgments:

RAS was supported by the National Natural Science Foundation of China–Natural Environment Research Council of the United Kingdom joint research program (41661134049 and NE/P013805/1), Second Tibetan Plateau Scientific Expedition and Research (2019QZKK0705), the National Natural Science Foundation of China joint research program of Yunnan (grant No. U1502231), NSFC-NERC (Natural

Environment Research Council of the UK) joint research program (No. 41661134049 and No. NE/P013805/1), and a XTBG International Fellowship for Visiting Scientists. Support also came from the National Natural Science Foundation of China (No. 31800183), Chinese Academy of Sciences 135 Program (No. 2017XTBG-T03), and CAS 'Light of West China' Program. We would like to thank Prof. Yuan, H. L. and Bao, Z. A. from State Key Laboratory of Continental Dynamics in Northwest University for dating experiment, Prof. Deng, C. L. from Institute of Geology and Geophysics of CAS and Prof. Tian Y. T. from Sun Yat-Sen University for reviewing and nice suggestions. Datasets for this research are included in this paper (Table 1) are available in Nutstore (https://www.jianguoyun.com/p/DUI6ngYQ_7KlCBjP_44D (Password: pcEKxu)) and its supplementary information file (Table S1) are also available in Nutstore (https://www.jianguoyun.com/p/DUFj3W0Q_7KlCBj0iIoD (Password：4xcmU3)). These data can be permanently seen by all Nutstore users.

References:

An, W., Hu, X., Garzanti, E., 2021. Wang, J.-G., Liu, Q.. New Precise dating of the India-Asia collision in the Tibetan Himalaya at 61 Ma. Geophys. Res. Lett., 48, e2020GL090641.

Boos, W.R., Kuang, Z.M., 2010. Dominant control of the South Asian monsoon by orographic insulation versus plateau heating. Nature, 7278, 463, 218-222.

Brown, R.W., 1962. Paleocene flora of the Rocky Mountains and Great Plains. United States Geological Survey Professional Paper, Washington. 1-106.

Clift, P.D., Blusztajn, J., Nguyen, A.D., 2006. Large-scale drainage capture and surface uplift in eastern Tibet–SW China before 24 Ma inferred from sediments of the Hanoi Basin, Vietnam. Geophys. Res. Lett., 33, L19403.

Clift, P.D., Carter, A., Wysocka, A., Hoang, V.L., Zheng, H., and Neubeck, N., 2020, A Late Eocene- Oligocene through-flowing river between the Upper Yangtze and South China Sea. Geochem. Geophy. Geosy., 21, e2020GC009046

Collinson, M.E., 1988. The special significance of the middle Eocene fruit and seed flora from Messel, West Germany. Cour Forsch-Inst Senckenberg. 107, 187-197.

Ding, L., Spicer, R.A., Yang, J., Xu, Q., Cai, F., Li, S., Lai, Q., Wang, H., Spicer, T.E.V., Yue, Y., Shukla, A., Srivastava, G., Khan., M.A., Bera, S., Mehrotra, R., 2017. Quantifying the rise of the Himalaya orogen and implications for the South Asian monsoon. Geology, 45, 215-218.

Favre, A., Packert, M., Pauls, S.U., Jahnig, S.C., Uhl, D., Michalak, I.N.A., Riehl, M., 2015. The role of the uplift of the Qinghai-Tibetan Plateau for the evolution of Tibetan biotas. Biol, Rev., 1, 90, 236-253.

Gilley, L.D., Harrison, T.M., Leloup, P.H., Ryerson, F.J., Lovera, O.M., Wang, J.H., 2003. Direct dating of left-lateral deformation along the Red River shear zone, China and Vietnam. J. Geophys. Res. - Sol. Earth., 108, B2, 2127.

Gourbet, L., Leloup, P.H., Paquette, J.L., Sorrel, P., Maheo, G., Wang, G.C., Xu, Y.D., Cao, K., Antoine, P.O., Eymard, I., 2017. Reappraisal of the Jianchuan Cenozoic basin stratigraphy and its implications on the SE Tibetan plateau evolution. Tectonophysics, 700-701, 162-179.

Herman, A.B., Spicer, R.A., Aleksandrova, G.N., Yang, J., Jin, J.H., 2017. Eocene–early Oligocene climate and vegetation change in southern China: Evidence from the Maoming Basin. Palaeogeogr., Palaeocl., Palaeoecol., 479, 126-137.Hoke, G.D., 2018. Geochronology transforms our view of how Tibet's southeast margin evolved. Geology, 46, 1, 95-96.

Hoskin, P.P., 2000. Patterns of chaos: fractal statistics and the oscillatory chemistry of zircon. Geochim. Cosmochim. AC, 64, 1905-1923.

Hu, H.H., Chaney R.W., 1940. A Miocene flora from Shantung Province, China. Carnegie Institution of Washington Publication. 507, 1-147.

Huang, J., Su, T., Jia, L.B., Spicer, T., Zhou, Z.K., 2018. A fossil fig from the Miocene of southwestern China: Indication of persistent deep time karst vegetation. Rev. Palaeobot. Palyno., 258, 133-145.

Huang, J., Shi, G.L., Su, T., Zhou Z.K., 2017. Miocene Exbucklandia (Hamamelidaceae) from Yunnan, China and its biogeographic and palaeoecologic implications. Rev. Palaeobot. Palyno., 244: 96-106.

Huang, J., Su, T., Lebereton-Anberree, J., Zhang, S.T., Zhou, Z.K., 2016a. The oldest Mahonia (Berberidaceae) fossil from East Asia and its biogeographic implications. J. Plant Res., 129, 2, 209-223.

Huang, Y., Jia, L., Wang, Q., Mosbrugger, V., Utescher, T., Su, T., Zhou, Z.K., 2016b. Cenozoic plant diversity of Yunnan: A review. Plant Diversity, 38, 6, 271-282.

Jin, J.H., Herman, A.B., Spicer, R.A., Kodrul, T.M., 2017. Palaeoclimate background of the diverse Eocene floras of South China. Sci. Bull., 62, 1501-1503.

Kapp, P., DeCelles, P.G., Gehrels, G.E., Heizler, M., Ding, L., 2007. Geological records of the Lhasa-Qiangtang and Indo-Asian collisions in the Nima area of central Tibet. Geol. Soc. Am. Bull., 119, 7-8, 917-933.

Lebreton-Anberrée, J., Li, S., Li, S.F., Spicer, R.A., Zhang, S.T., Su, T., Deng, C.L., Zhou, Z.K., 2016. Lake geochemistry reveals marked environmental change in Southwest China during the Mid Miocene Climatic Optimum. Sci. Bull., 61,11, 897-910.

Li, S.F., Mao, L.M., Spicer, R.A., Lebreton-Anberrée, J., Su, T., Sun, M., Zhou, Z.K., 2015. Late Miocene vegetation dynamics under monsoonal climate in southwestern China. Palaeogeogr, Palaeocl., Palaeoecol., 425, 14-40.

Li, S.H., Su, T., Spicer, R.A., Xu, C.L., Sherlock, S., Halton, A., Hoke, G.D., Tian, Y.M., Zhang, S.T., Zhou, Z.K., Deng, C.L., Zhu, R.X., 2020a. Oligocene deformation of the Chuandian Terrane in the SE margin of the Tibetan Plateau related to the extrusion of the Indochina. Tectonics, 39, e2019TC005974.

Li, S.H., van Hinsbergen, D.J.J., Najman, Y., Jing, L.Z., Deng, C., Zhu, R., 2020b. Does pulsed Tibetan deformation correlate with Indian plate motion changes? Earth Planet. Sc. Lett., 536, 116-144.

Liu, Y.S., Hu, Z.C., Zong, K.Q., Gao, C.G., Gao, S., Xu, J., Chen, H.H., 2010. Reappraisement and refinement of zircon U-Pb isotope and trace element analyses by LA-ICP-MS. Chinese Sci. Bull., 55, 15, 1535-1546.

Linnemann, U., Su, T., Kunzmann, L., Spicer, R.A., Ding, W.N., Spicer, T.E.V., Zieger, J., Hofmann, M., Moraweck, K., Gärtner, A., Gerdes, A., Marko, L., Zhang, S.T., Li, S.F., Tang, H., Huang, J., Mulch, A., Mosbrugge, V., Zhou, Z.K., 2017. New U-Pb dates show a Paleogene origin for the modern Asian biodiversity hot spots. Geology, 46, 1, 3-6.

Lu, L.M., Mao, L.F., Yang, T., Ye. J.F., Liu, B., Li, H.L., Sun, M., Miller, J.T., Mathews, S., Hu, H.H., Niu, Y.T., Peng, D.X., Chen, Y.H., Smith, S.A., Chen, M., Xiang, K.L., Le, C.T., Dang, V.C., Lu, A.M., Soltis, P.S., Soltis, D .E., Li, J.H., Chen, Z.D., 2018. Evolutionary history of the angiosperm flora of China. Nature, 554, 7691, 234-238.

Ma, H.J., 2013. Cenozoic Stratigraphy and Paleoenvironmental Changes in the Hengduan Mountains Region, Southwest China. Kunming University of Science and Technology., Kunming, China.

Meng, H.H., Jacques, F.M.B., Su, T., Huang, Y.J., Zhang, S.T., Ma, H.J., Zhou, Z.K., 2014. New Biogeographic insight into Bauhinias.l. (Leguminosae): integration from fossil records and molecular analyses. BMC Evol. Biol., 14, 181.

Molnar, P., Boos, W.R., Battisti, D.S., 2010. Orographic controls on climate and paleoclimate of Asia: Thermal and mechanical roles for the Tibetan Plateau. Annu. Rev. Earth Planet. Sc. Lett., 38, 77-102.

Molnar, P., Tapponnier, P., 1975. Cenozoic Tectonics of Asia: Effects of a Continental Collision: Features of recent continental tectonics in Asia can be interpreted as results of the India-Eurasia collision. Science, 189, 4201, 419-426.

Myers, N., Mittermeier, R.A., Mittermeier, C.G., da Fonseca, G.A.B., Kent. J., 2000. Biodiversity hotspots for conservation priorities. Nature, 403, 6772, 853-858.

Ren, J. S., Wang, Z. X., Chen, B, W., Jiang, C. F., Niu, B. G., Li, J. T., Xie, G. L., He, Z. J., Liu, Z. G., 1997. A new generation tectonic map of China. Geol. Bull. China, 16, 3, 225-248.

Renner, S.S., 2016. Available data point to a 4-km-high Tibetan Plateau by 40 Ma, but 100 molecular-clock papers have linked supposed recent uplift to young node ages. J. Biogeogr., 43, 8, 1479-1487.

Schärer, U., Zhang, L. S., Tapponnier, P., 1994. Duration of strike-slip movements in large shear zone: the Red River belt, China. Earth Planet. Sc. Lett., 126, 379-397

Spicer, R.A., Farnsworth, A., Su, T., 2020a. Cenozoic Topography, Monsoons and Biodiversity Conservation within the Tibetan Region: An Evolving Story. Plant Diversity, 4, 229-254, https://doi.org/10.1016/j.pld.2020.06.011.

Spicer, R.A., Su, T., Valdes, P.J., Farnsworth, A., Wu, F.-X., Shi, G., Spicer, T.E.V., Zhou, Z.-K., 2020b. Why the 'uplift of the Tibetan Plateau' is a myth. Natl. Sci. Rev., 8, nwaa91.

Spicer, R.A., Yang, J., Herman, A., Kodrul, T., Aleksandrova, G., Maslova, N., Spicer, T., Ding, L., Xu, Q., Shukla, A., Srivastava, G., Mehrotra, R., Liu, X.Y., Jin, J.H., 2017. Paleogene monsoons across India and South China: Drivers of biotic change. Gondwana Res., 49, 350-363.

Su, T., Spicer, R.A., Li, S.H., Xu, H., Huang, J., Sherlock, S., Huang, Y.J., Li, S.F., Wang, L., Jia, L.B., Deng, W., Liu, J., Deng, C., Zhang, S.T., Valdes, P.J., Zhou, Z.K., 2019. Uplift, climate and biotic changes at the Eocene-Oligocene transition in south-eastern Tibet. Natl. Sci. Rev., 6, 3, 495-504.

Tapponnier, P., Peltzer, G., Dain, A.Y.L., Armijo, R., Cobbold, P., 1982. Propagating extrusion tectonics in Asia: New insights from simple experiments with plasticine. Geology, 10, 12, 611-616.

Wang, S.M., Li, J.R., 1991. Lacustrine sediments- an indicator of historical climatic variations—The case of Qinghai Lake and Daihai Lake. Chinese Sci. Bull., 36, 16, 1364-1368.

Wang, Q., Zhang, P.Z., Freymueller, J.T., Bilham, R., Larson, K.M., Lai, X.A., You, X.Z., Yang, Z.J., Chen, Q.Z., 2001. Present-day crustal deformation in China constrained by global positioning system measurements. Science, 294, 5542, 574-577.

Wiedenbeck, M., Hanchar, J.M., Peck, W.H., Sylvester, P., Valley, J., Whitehouse, M., Kronz, A., Morishita, Y., Nasdala, L., Fiebig, J., Franchi, I., Girard, J.-P., Greenwood, R.C., Hinton, R., Kita, N., Mason, P.R.D., Norman, M., Ogasawara, M., Piccoli., P.M., Rhede, D., Satoh, H., Schulz-Dobrick, B., Skår, Ø., Spicuzza, M.J., Terada, K., Tindle, A., Togashi, S., Vennemann, T., Xie, Q. and Zheng, Y.-F. 2004. Further characterisation of the 91500 zircon crystal. Geostand. Geoanal. Res., 28, 9-39.

Wu, Z.Y., Zhou, Z.K., Sun, H., Li, D.Z., Peng, H., 2006. The areal-types of seed plants and their origin and differentiation. Yunnan Publishing Group Corporation Yunnan Science & Technology Press. Kunming, China. 12-145

Wu, Z.Y., Zhu, Y., Jiang, H., 1987. Vegetation of Yunnan. Science Press. Beijing, China. 81-714

Yan, Y., Carter, A., Huang, C.Y., Chan, L.S., Hu, X.Q., Lan, Q., 2012. Constraints on Cenozoic regional drainage evolution of SW China from the provenance of the Jianchuan Basin. Geochem. Geophy. Geosy., 13, 3, Q03001.

Yao, Y.F., Bera, S., Ferguson, D.K., Mosbrugger, V., Paudayal, K.N., Jin, J.H., Li, C.S., 2009. Reconstruction of paleovegetation and paleoclimate in the Early and Middle Eocene, Hainan Island, China. Climatic Change, 92, 1, 169-189.

Yunnan Bureau of Geology and Mineral Resources (YBGMR), 1990. Regional Geology of Yunnan Province. Beijing.

Yin, A., Harrison, T.M., 2000. Geologic Evolution of the Himalayan-Tibetan Orogen. Annu. Rev. Earth Pl. Sc., 28, 1, 211-280.

Zachos, J., Pagani, M., Sloan, L., Thomas, E., Billups, K., 2001. Trends, rhythms, and aberrations in global climate 65 Ma to present. Science, 292, 5517, 686-693.

Zhang, K.X., Wang, G.C., Luo, M.S., Ji, J., Xu, Y.D., Chen, R.M., Chen, F.N., Song, B.W., Liang, Y.P., Zhang, J.Y., Yang, Y.F., 2010. Evolution of Tectonic Lithofacies Paleogeography of Cenozoic of Qinghai-Tibet Plateau and Its Response to Uplift of the Plateau. Earth Sci.: J. China U. Geosci., 35, 5, 697-712.

Zheng H., Clift, P.D., He, M., Bian, Z., Liu, G., Liu, X., Xia, L., Yang, Q., Jourdan, F., 2020. Formation of the First Bend in late Eocene gave birth to the Modern Yangtze River. Geology, 49, 35-39

Zhou, Z.K., Wang, T.X., Huang, J., Liu, J., Deng, W., Li, S., Deng, C., Su, T., 2020. Fossil leaves of Berhamniphyllum (Rhamnaceae) from Markam, Tibet and their biogeographic implications. Sci. China Earth Sci., 63, 224-234.

Figures and Tables:

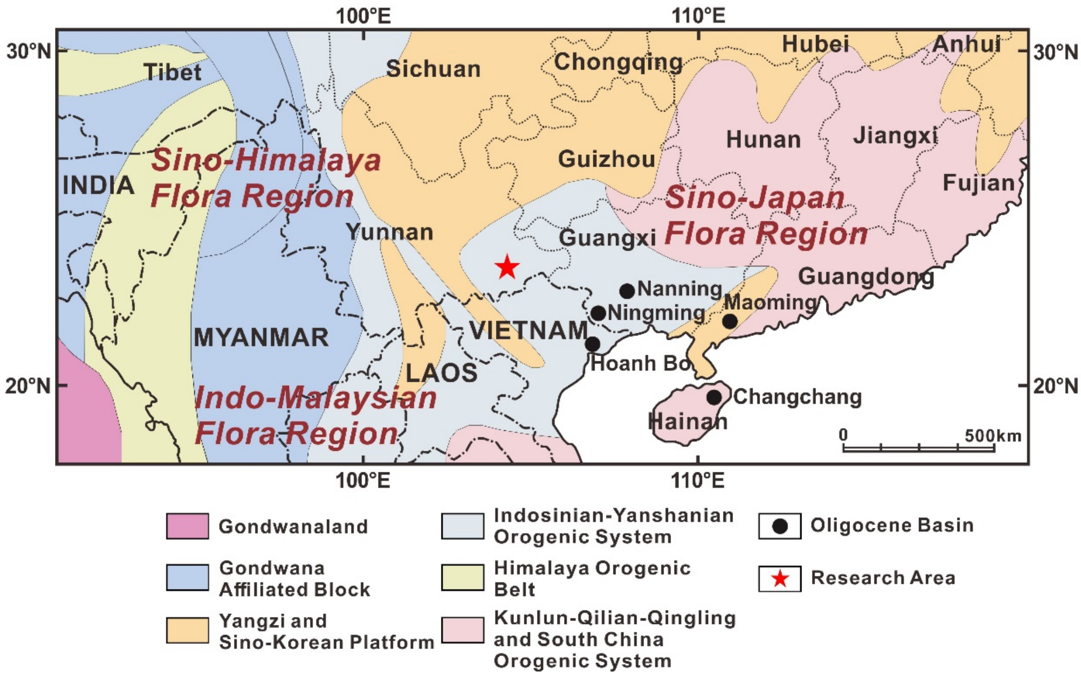

Fig. 1. Geotectonic map of southern China and adjacent regions showing typical Oligocene basins with plant fossils in South China and Vietnam (Geotectonic source from Ren et al., 1997).

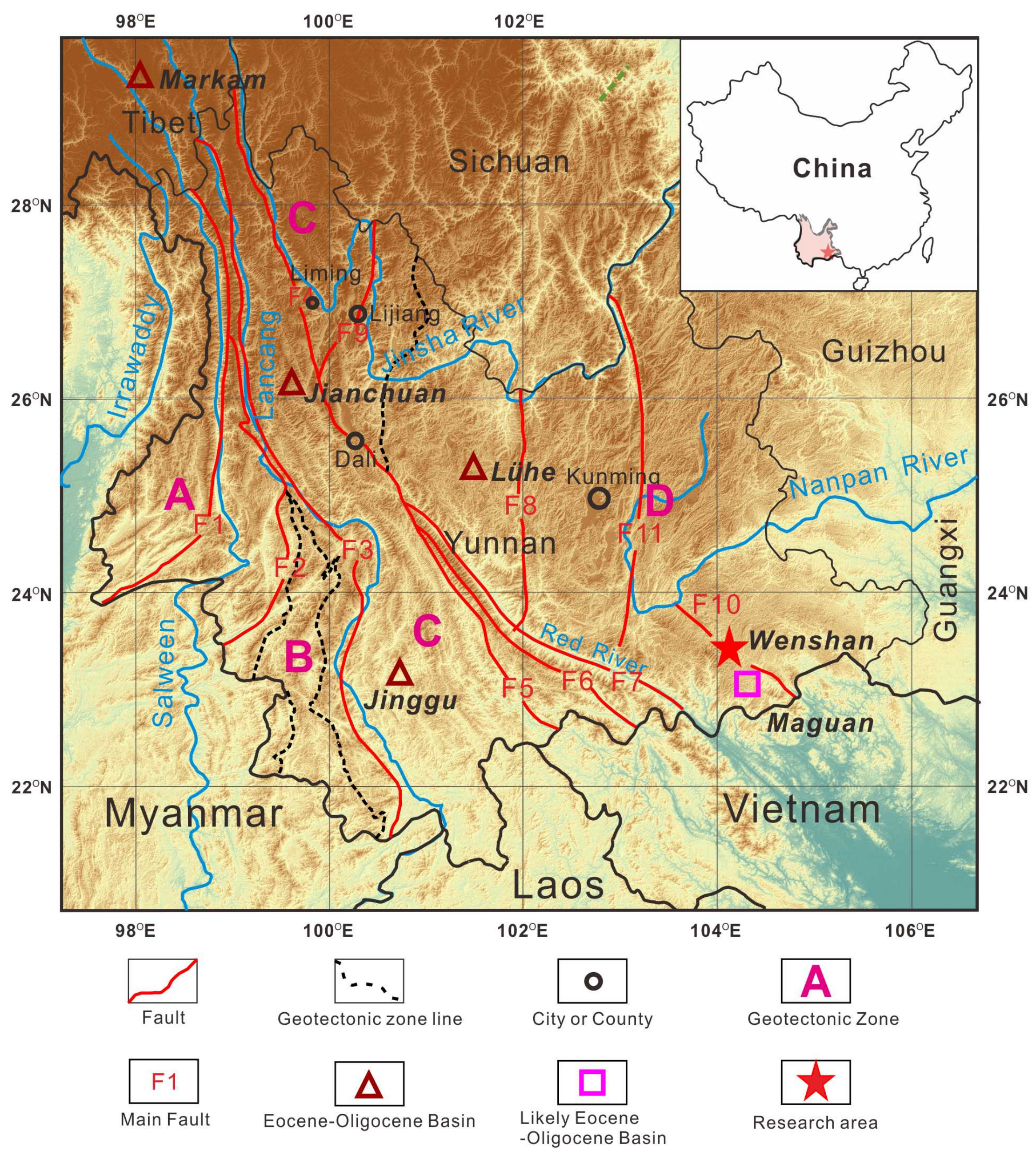

Fig. 2. Location map of late Eocene-early Oligocene sedimentary basins, geological units and main rivers of Yunnan Province and adjacent region (Geological units from Yunnan Bureau of Geological Survey, 2014) (Topographic map from Shuttle Radar Topography Mission of United States Geological Survey https://earthexplorer.usgs.gov/). Abbreviations: **F1** = Nu River Fault; **F2** = Kejie Fault; **F3** = Lancang River Fault; **F4** = Jinsha River Fault; **F5** = Amojiang Fault; **F6** = Ailao Shan Fault; **F7** = Red River Fault; **F8** = Yuanmou-Lvzhi River Fault; **F9** = Xiaojinhe Fault; **F10** = Wenshan-Malipo Fault; **F11** = Xiaojiang Fault **A** =

Gangdese-Himalayan orogen zone; **B** = Sibamasu and the Qamdo Block; **C** = Qiangtang-Salween River-Lancang River- Jinsha River orogen zone; **D** = the upper Yangtze ancient continent.

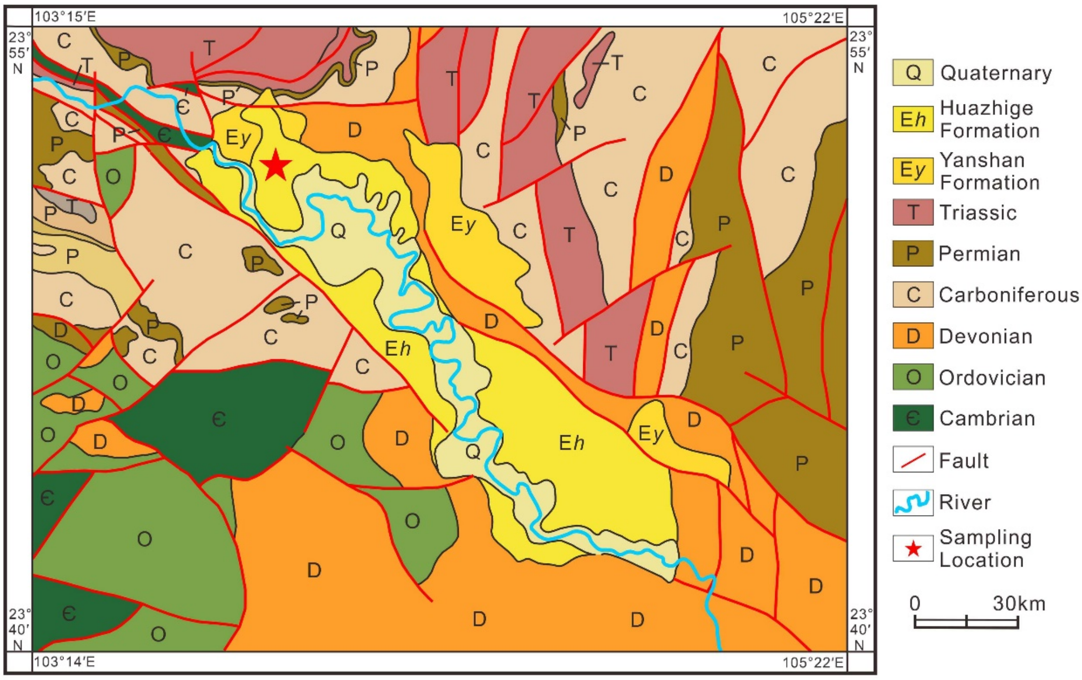

Fig.3. Geological map of the Wenshan Basin area and sampling position of the volcanic ashes (source from YBGMR, 1990)

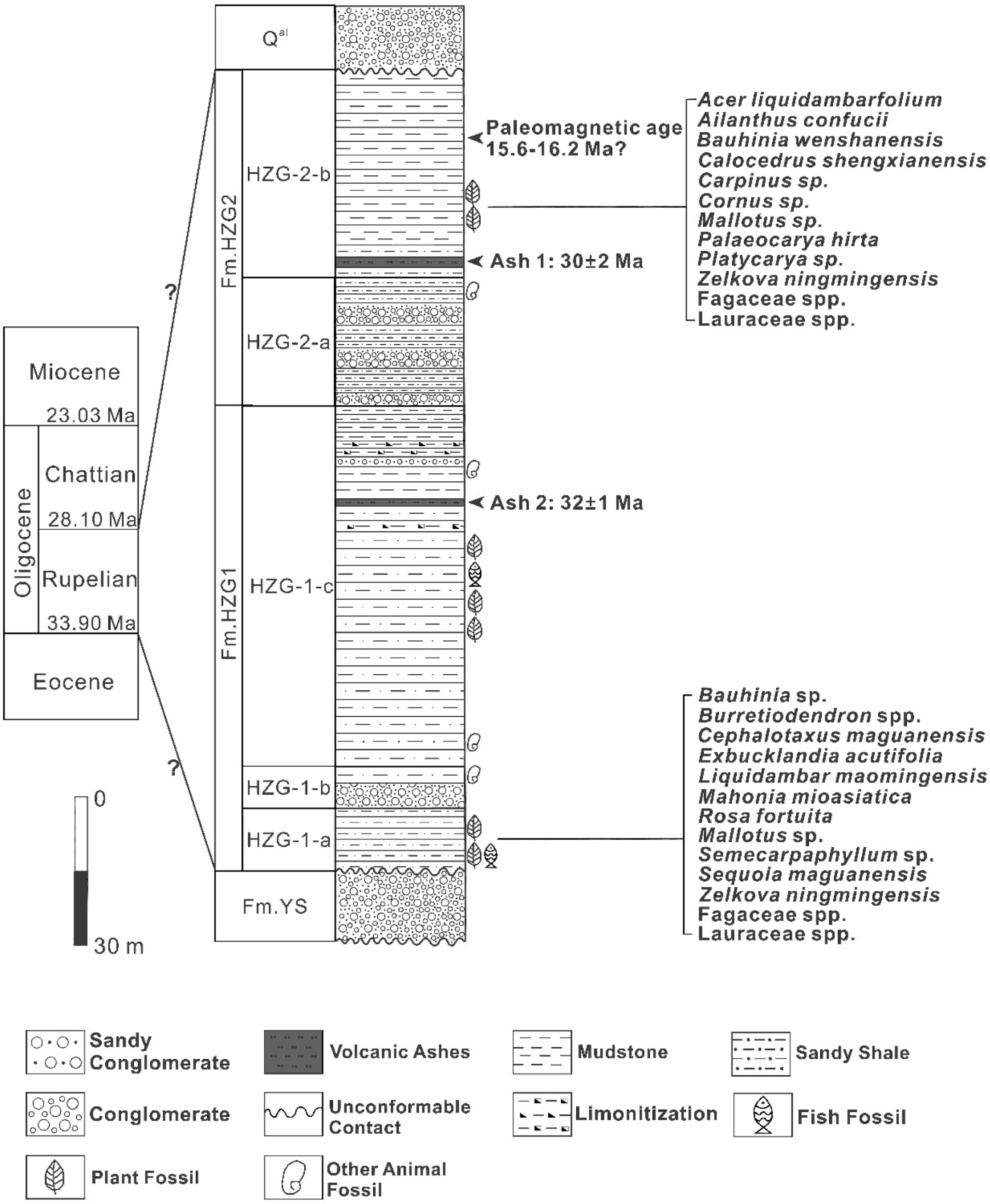

Fig. 4. Graphical summary of the sampling succession on the north of Wenshan basin. All the zircon grains were collected from ‘Ash 1’ and ‘Ash 2’, and paleomagnetic data (According to Lebreton-Anberrée et al., 2016) overlies the volcanic ash beds. Abbreviations: Fm. HZG = Huazhige Formation; Fm. YS = Yanshan Formation

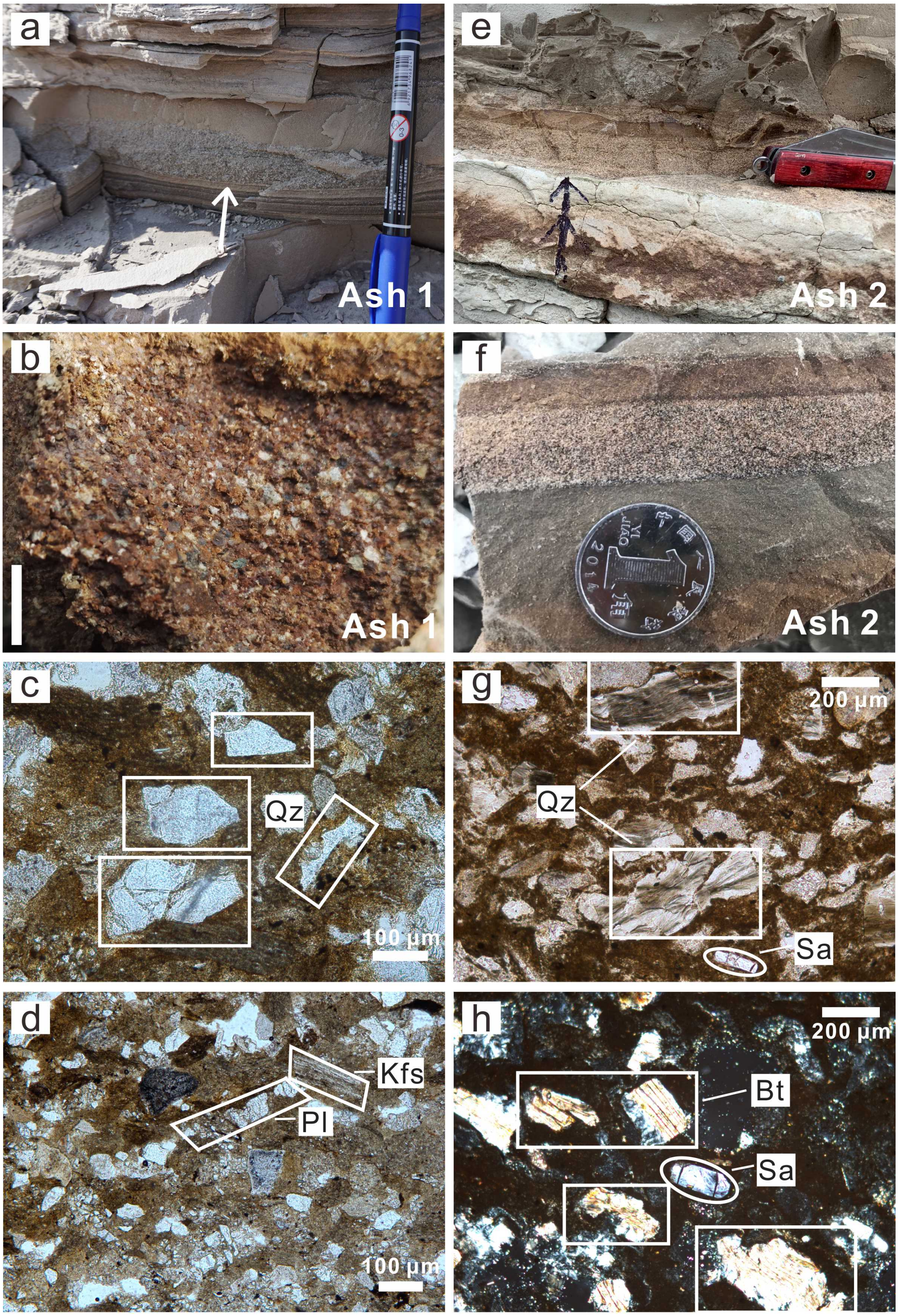

Fig. 5. Field photos of outcrop with the volcanic ashes and microphotographs of minerals with volcanic features. **a, b, c, d.** 'Ash 1'; **e, f, g, h.** 'Ash 2'; **c, d, g, h.** microphotographs of

ashes; **g.** cross – polarized light; **b.** an increase in grain sizes towards the middle of the ash lens and fining thereafter. Note angularity and large size of the grains (~ 3 mm diameter) in the center of the lens. Abbreviations: **Qz** = quartz; **Kfs** = K-feldspar; **Pl** = plagioclase; **Sa** = sanidine; **Bt** = biotite. Scale bars of **b** = 1 cm.

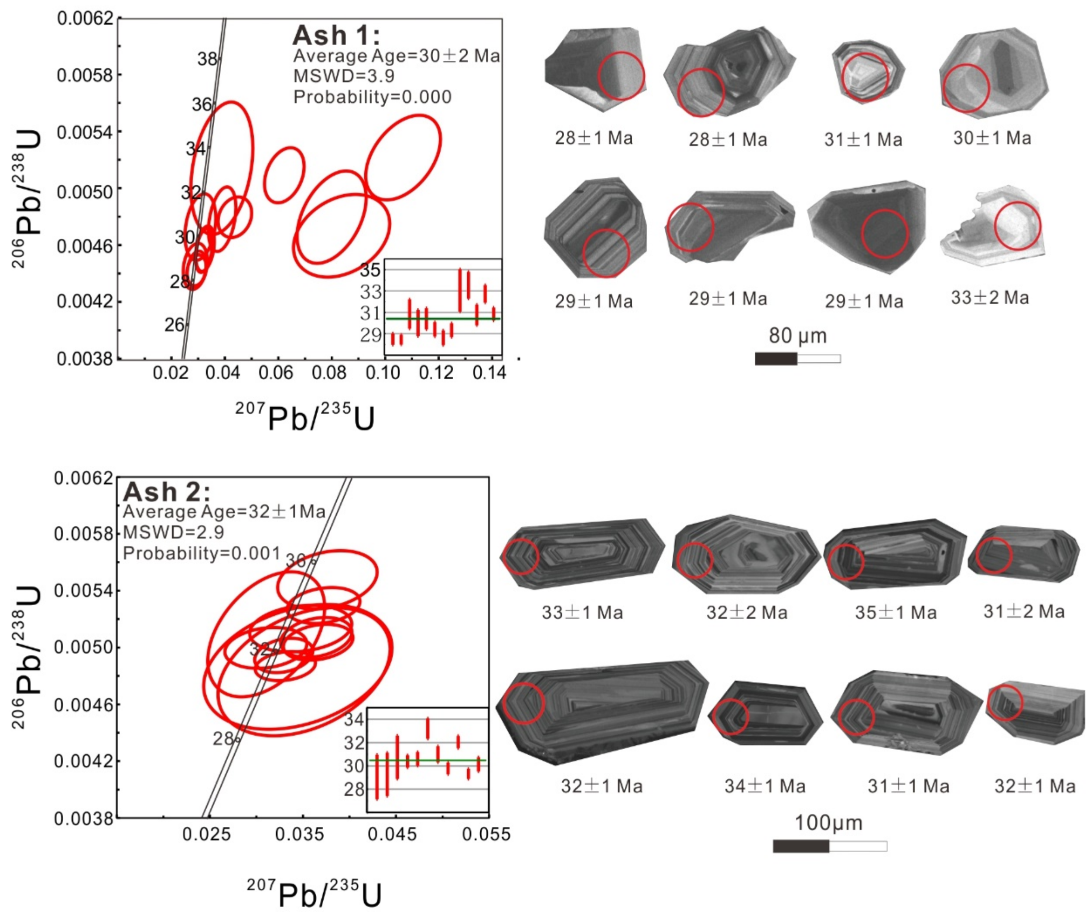

Fig. 6. Concordia diagrams and CL images of zircon grains with laser spot locations for the $^{206}Pb/^{238}U$ ages from the Wenshan volcanic ashes.

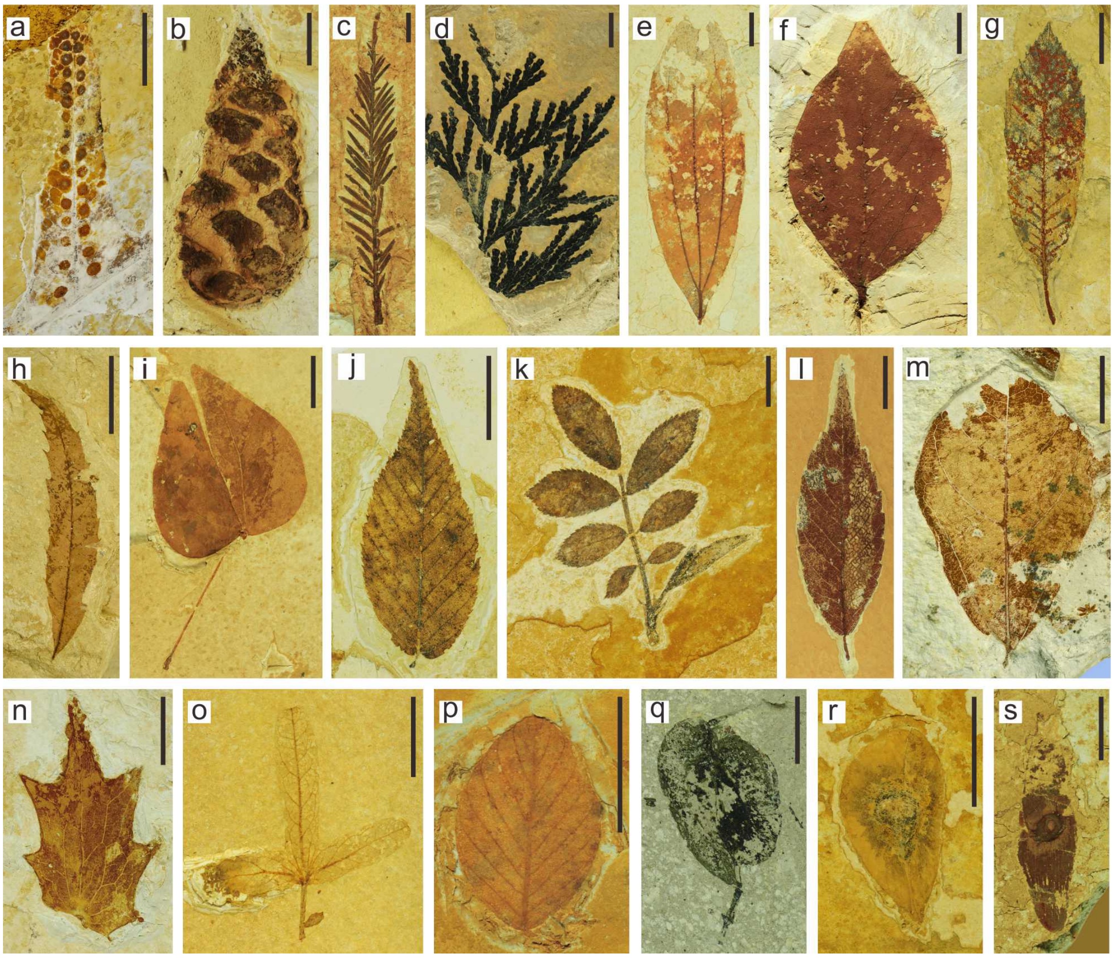

Fig. 7. Representative taxa from Wenshan flora. **a.** *Goniophlebium macrosorum* C.L.Xu et Z.K. Zhou; **b.** *Pinus massoniana* Lambert.; **c.** *Sequoia maguanensis* J.W. Zhang et Z.K. Zhou; **d.** *Calocedrus shengxianensis* (He, Sun et Liu) J.W. Zhang et Z.K. Zhou; **e.** *Cinnamomum cf. burmannii* (C. G. et Th. Nees) Bl.; **f.** *Exbucklandia acutifolia* J. Huang et Z. K. Zhou; **g.** Quercus sp.; **h.** *Berryophyllum yunnanense* (Colani) Z.K. Zhou; **i.** *Bauhinia wenshanensis* H.H. Meng et Z.K.Zhou; **j.** *Carpinus* sp.; **k.** *Rosa fortuita* T. Su et Z.K. Zhou; **l.** *Zelkova* sp.; **m.** *Ficus microtrivia* J. Huang et Z.K. Zhou; **n.** *Mahonia mioasiatica* J. Huang et Z.K. Zhou; **o.** *Palaeocarya hispida* H.H. Meng & Z.K. Zhou; **p.** *Berhamniphyllum miofloribundum* (Hu et Chaney) J. Huang, T. Su et Z.K. Zhou; **q.** *Ulmus prelanceaefolia* Q.Y. Zhang et Y.W. Xing; **r.** *Burretiodendron parvifructum* J. Lebreton Anberrée et Z.K. Zhou; **s.** *Ailanthus confucii* Unger. Scale bar = 1 cm

Table 1. Composition of the Wenshan palaeolora with compared with the modern flora of the region.

Wenshan Flora		Present or absent in modern Yunnan
Family	Genus	
Polypodiaceae	*Goniophlebium*	Present
Pinaceae	*Pinus*	Present
Cupressaceae	*Sequoia*	Absent
Cupressaceae	*Calocedrus*	Present
Lauraceae	*Cinnamomum*	Present
Berberidaceae	*Mahonia*	Present
Hamamelidaceae	*Exbucklandia*	Present
Fabaceae	*Bauhinia*	Present
Fagaceae	*Quercus*	Present
Juglandaceae	*Palaeocarya*	Present
Betulaceae	*Carpinus*	Present
Rosaceae	*Rosa*	Present
Rhamnaceae	*Berchemiphyllum*	Present
Ulmaceae	*Ulmus*	Present
Ulmaceae	*Zelkova*	Present
Moraceae	*Ficus*	Present
Malvaceae	*Burretiodendron*	Present
Simaroubaceae	*Ailanthus*	Present
Note: Arranged according to APG IV; Modern flora data are from (Wu et al., 1987).		